

Electronic Supplementary Information for

Formate Adsorption on Pt Nanoparticles during Formic Acid Electro-oxidation: Insights from In Situ Infrared Spectroscopy

Ian J. McPherson,[†] Philip A. Ash,[†] Robert M. J. Jacobs,[‡] Kylie A. Vincent,[†]*

[†]Department of Chemistry, University of Oxford, Inorganic Chemistry Laboratory, South Parks Road, Oxford, OX1 3QR, UK

[‡]Department of Chemistry, University of Oxford, Chemistry Research Laboratory, 12 Mansfield Road, Oxford, OX1 3TA, UK

Table of Contents

S1. Challenges Associated with in situ IR Spectroelectrochemistry in Formic Acid

S2. Experimental Methods

Figure S1. An SEM cross section through a typical Pt/C film cast onto a silicon wafer.

S3. Demonstration of Effective Potential Control and Mass Transport in the ATR-IR Cell

Figure S2. Comparison of cyclic voltammograms for comparable catalyst layers on a rotating disc electrode and in the ATR-IR cell.

Figure S3 Control experiments on layers comprising only carbon black, studied using ATR-IR spectroelectrochemistry.

Figure S4 A comparison between in situ spectra obtained in unlabeled and ¹³C-labeled HCOOH solutions during cyclic voltammetry.

S4 Data handling

Figure S5 Single beam spectra showing the bipolar nature of the CO peak

Figure S6 Examples of fits to the 1315 and ca 1250 cm⁻¹ peaks and a comparison of fitting versus using the maximum absorbance to analyse the 1315 cm⁻¹ potential dependence

Supplementary References

S1. Challenges Associated with *in situ* IR Spectroelectrochemistry in Formic Acid

Complications can arise in the interpretation of spectra if the supporting electrode or electrode underlayer is susceptible to adsorption of species present during the reaction. One reason that adsorbed CO has been well studied is that it does not strongly adsorb on Au, allowing Au electrodes to be used as supports,^[1] although CO can still be observed to some degree in the spectra.^[2] Other intermediates adsorb more strongly on Au. Formate, an intermediate observed in formic acid and methanol oxidation, adsorbs strongly on Au, Pt and Pd.^[3–5]

To avoid interference from species adsorbed on the supporting electrode, relatively inert carbon electrodes can be used (for example glassy carbon).^[6] However, to date such electrodes have only been used in IRAS configurations, which involve a thin-layer electrochemical cell to minimise IR absorption from the aqueous electrolyte and thereby often suffer from limited mass transport to/from the catalyst.^[7] Changing composition of the thin layer over time during catalysis can lead to re-adsorption of side products and misleading conclusions about the nature of the reaction.^[8,9]

S2. Experimental Methods

Catalyst ink (25 mg mL⁻¹) was prepared by ultrasonically dispersing carbon-supported Pt catalyst (Pt/C, 60 wt.% Pt on Vulcan XC72 carbon, HiSPEC 9000, Alfa Aesar) in ethanol (puriss, Sigma Aldrich). Catalyst layers in the ATR-IR cell were prepared by drop casting 10 µL ink onto a silicon internal reflection element (IRE) (ca 5 x 8 x 1 mm³, 5 reflections, Crystal GmbH). The thickness of catalyst layers produced in this way were studied by scanning electron microscopy. A cross section was obtained by casting a film onto a silicon wafer (Crystal GmbH) and snapping the wafer in half. The wafer was then imaged using a Jeol 840F scanning electron microscope operated at 5 kV (Figure S1). Using this method a typical film was found to be 1-2 µm thick, similar to the penetration depth of the IR evanescent wave.

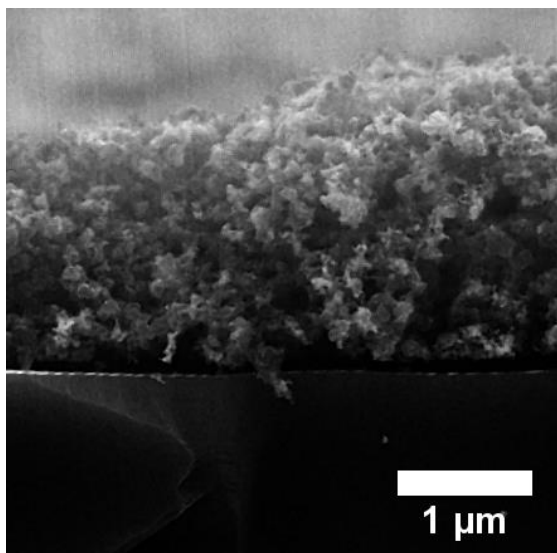


Figure S1. An SEM cross section through a typical Pt/C film cast onto a silicon wafer.

A fast curing silicone (SE4486CV, Dow Corning) was used to seal the IRE into a polyether ether ketone (PEEK) baseplate. The baseplate was mounted in an ATR accessory (GladiATR, PIKE Technologies), modified to allow multiple reflections. A sheet of carbon paper (TGP-H-030, Toray Industries, Inc.) was placed over the catalyst layer and pressed down by a carbon flow field (Figure 1). The carbon flow field was manufactured in house and consists of a polished pyrolytic graphite plate (Momentive Performance Materials Inc.) with a central inlet and a radial array of outlet holes to allow the flow of solution over the film during experiments. An additional hole in the flow field allows positioning of the Luggin capillary of the reference electrode compartment close to the catalyst film to minimize the uncompensated resistance. The flow field was totally encapsulated in epoxy resin, except for the bottom face, to minimize the amount of carbon in contact with solution. The flow field was housed in a PEEK body, designed and built in-house, which also positions a Pt gauze ring counter electrode in the path of the solution outlet and contains a reference electrode compartment for a silver/silver chloride electrode (BAS Inc.). The cell body seals onto the baseplate using a Viton O ring.

For rotating disc electrochemistry (RDE) experiments, the same Pt/C catalyst was dispersed in a mixture of Nafion (perfluorinated resin, aqueous dispersion 10 wt% in H₂O, Sigma Aldrich), MilliQ water, isopropanol (puriss. Sigma Aldrich) to 1:300:100 by volume and 10 μL of this ink was deposited onto a homemade 7 mm diameter glassy carbon (Alfa Aesar) rotating disc electrode and dried in air. Nafion was incorporated into the catalyst layer for RDE experiments to produce a stable electrode structure.

Nafion was not used in the IR spectroelectrochemical experiments on the catalyst layer because it can contribute IR absorption in the low wavenumber region which may mask adsorbates. It was found that the dried catalyst layers were stable in the ATR-IR setup, possibly aided by the carbon paper layer pressed down by the flow field.

All potentials were measured relative to a silver/silver chloride electrode (3 M NaCl) at room temperature and are reported with respect to the standard hydrogen electrode using ($E_{\text{SHE}} = E_{\text{Ag}/\text{AgCl}} + 0.209 \text{ V}$).^[10] Electrochemical control was provided by a potentiostat (μAutolab, Metrohm) and IR spectra were recorded using an FTS7000 FTIR spectrometer (Bio-Rad) with a liquid nitrogen-cooled HgCdTe detector. The onset of spectral data collection was triggered by the potentiostat to ensure accurate timing. Spectra were acquired every 1 s at a resolution of 4 cm⁻¹ and co-added as specified. Solutions were prepared using MilliQ water (18.2 MΩ cm, Millipore), HClO₄ (for analysis, Acros) and HCOOH (puriss. p.a., Fluka) or ¹³C-labeled HCOOH (99% ¹³C, Cambridge Isotope Laboratories, Inc.).

S3. Demonstration of Effective Potential Control and Mass Transport in the ATR-IR Cell

Cyclic voltammetry of a Pt/C catalyst layer in HCOOH solution was used to compare the potential control and mass transport in the ATR-IR cell to that on a rotating disc electrode (RDE). The same amount of Nafion-containing catalyst ink was cast on the IRE in the ATR-IR cell, and on a glassy carbon rotating disc electrode (RDE). The surface areas of the RDE and IRE are very similar (40 mm² and 38.5 mm², respectively) and therefore provide comparable catalyst layers. The catalyst layers were cleaned before use by cycling between 0.0 V and 1.2 V vs

SHE until a stable voltammogram was obtained. Cyclic voltammograms recorded at 10 mV s^{-1} in 10 mM HCOOH and 0.5 M HClO_4 solution are shown in Figure S2 for the ATR-IR cell with solution flowing at 3 mL min^{-1} and with the RDE rotating at 500 rpm. The electrocatalytic features of the voltammograms at each electrode are similar in terms of the onset potential for formic acid oxidation, the current peaks, and the behaviour at high potential, indicating similar electrochemical control over the catalyst and mass transport in each case.

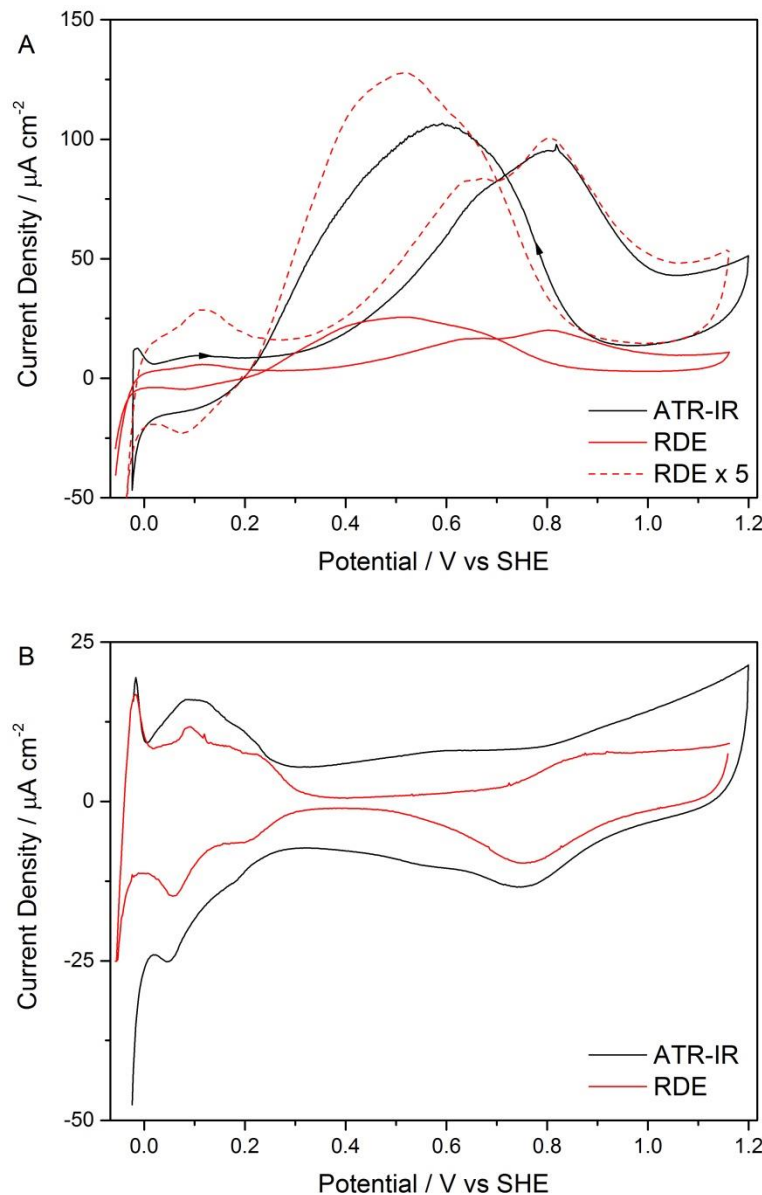


Figure S2. Comparison of cyclic voltammograms (scan rate 10 mV s^{-1}) for comparable catalyst layers (see text) operating in (A) $10 \text{ mM HCOOH} + 0.5 \text{ M HClO}_4$. Flow rate in ATR-IR cell 3 mL min^{-1} , RDE rotation rate 500 rpm. The RDE current density has been multiplied by 5 for

comparison with the ATR-IR cell current density. The scan direction is shown by arrows. (B) Cyclic voltammograms in 0.5 M HClO₄. Note that the same peaks are present in both the RDE and ATR-IR cell voltammograms, although they are slightly more pronounced at the RDE, due in part to the larger capacitive background current in the ATR-IR cell. Current densities, based on the electrochemical surface area determined through hydrogen desorption measurements, were lower in the RDE measurement presumably due to differences in mass transport in the different cell geometries.

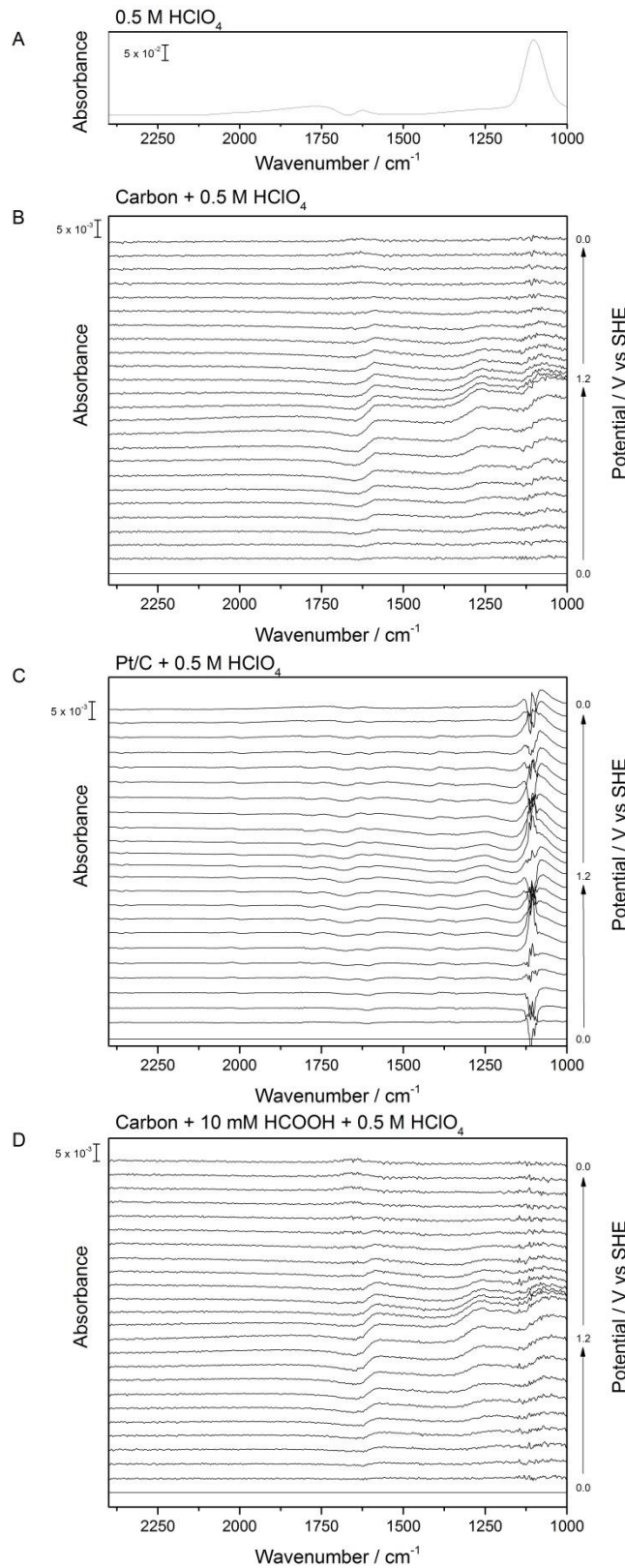


Figure S3 Control experiments on different components of the catalyst layer. A: 0.5 M HClO_4 solution. Background: Water. B: Carbon support film + 0.5 M HClO_4 during potential sweep from 0.0 V to 1.2 V at 10 mV s^{-1} . Background: First spectrum at 0.0 V in set. C: Pt/C catalyst layer + 0.5 M HClO_4 during potential sweep from 0.0 V to 1.2 V at 1 mV s^{-1} . Background: First spectrum at 0.0 V in set. D: Carbon support material + 10 mM HCOOH + 0.5 M HClO_4 during potential sweep from 0.0 V to 1.2 V at 1 mV s^{-1} . Background: First spectrum at 0.0 V in set. Carbon black inks were prepared by dispersing Vulcan XC72R in a mixture of Nafion (perfluorinated resin, aqueous dispersion 10 wt. % in H_2O , Sigma Aldrich), water, isopropanol (puriss. Sigma Aldrich) to 1:300:100 by volume. Nafion was used to aid dispersion of the carbon material.

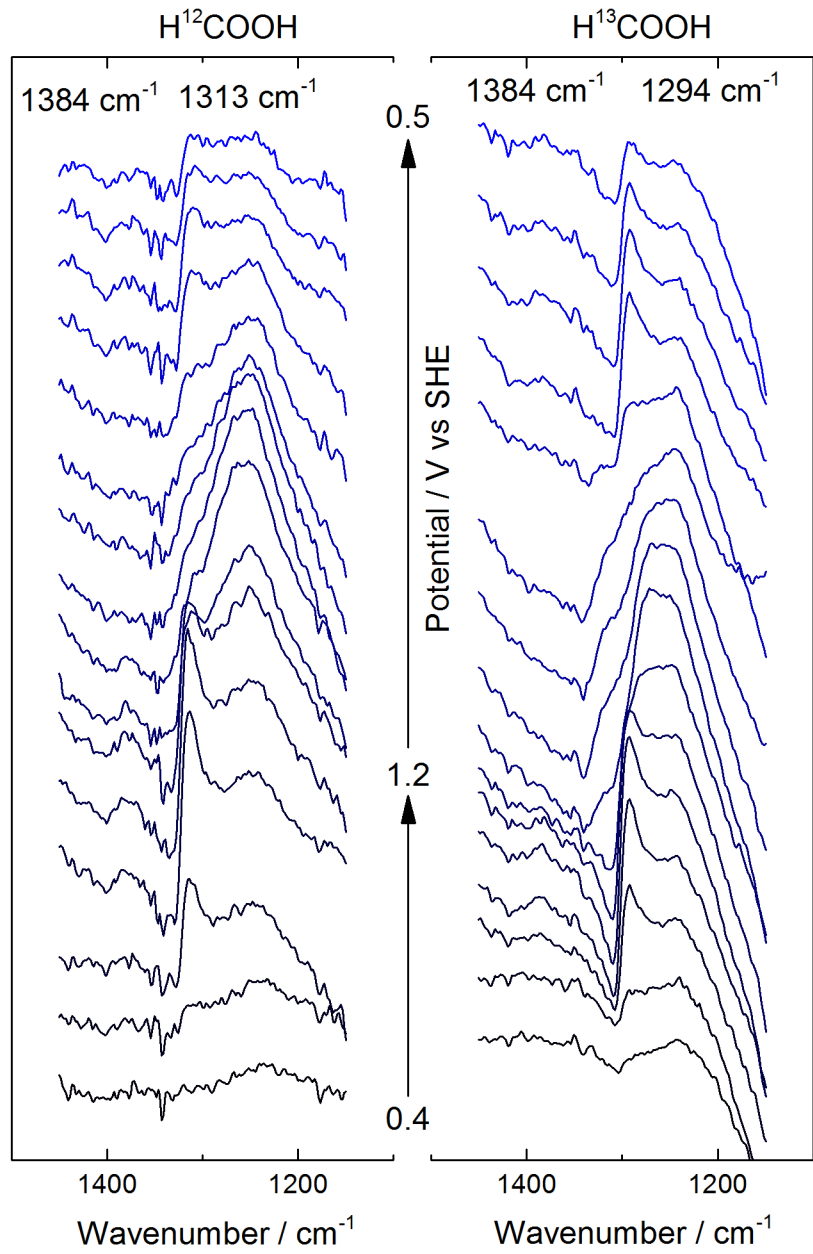


Figure S4 A comparison between in situ spectra obtained in unlabeled and ^{13}C -labeled HCOOH solutions during cyclic voltammetry. A: Spectra recorded in unlabeled HCOOH (10 mM). B: Spectra recorded in ^{13}C -labeled HCOOH (10 mM). Backgrounds obtained at 0.15 V during the cycle.

S4 Data handling

Infrared spectra of rough electrode surfaces often show abnormal peak shapes, manifesting as inverse (decrease in absorbance) or bipolar (both an increase and decrease in absorbance) peaks. These effects are not to be confused with the appearance of bipolar peaks produced by processing a spectrum with a background containing the same peak but at a slightly different position. The inherently bipolar nature of the CO peak observed in Figure 2 can be seen by inspecting single beam spectra recorded before and after adding HCOOH (Figure S5). The magnitude of the CO peak absorption is such that it clearly stands out in the single channel spectrum, showing as a significant dip in response at lower wavenumber (corresponding to the conventional, expected increase in absorption, see panel B), while a significant increase in response at higher wavenumber is observed (corresponding to the negative lobe in panel B). To quantify the amount of CO present we therefore opted to take the maximum positive absorbance in the region 2035-2046 cm^{-1} (noting that the position of the maximum changes with potential consistent with the expected Stark tuning).

The 1315 cm^{-1} peak also shows evidence of being bipolar, however uncertainty in the baseline makes this difficult to quantify. The peak's appearance as a shoulder on the larger ca 1250 cm^{-1} peak means that fitting is the preferred method to quantify it. We used Gaussian functions to fit both peaks and derive the 1315 cm^{-1} intensity reported in Figure 3C; examples of the fits, at two representative potentials, are shown in Figure S6A and S6B. For comparison the peak was also quantified by taking the maximum positive absorbance, as carried out for the CO peak. While the trend is almost identical for the majority of potentials examined, the presence of the ca 1250 cm^{-1} peak at higher potentials complicates analysis and results in larger relative values of the absorbance (Figure S6B). We thus feel that the intensity derived from fitting as a unipolar peak provides a more representative indication of the amount of formate than that derived from the absorbance.

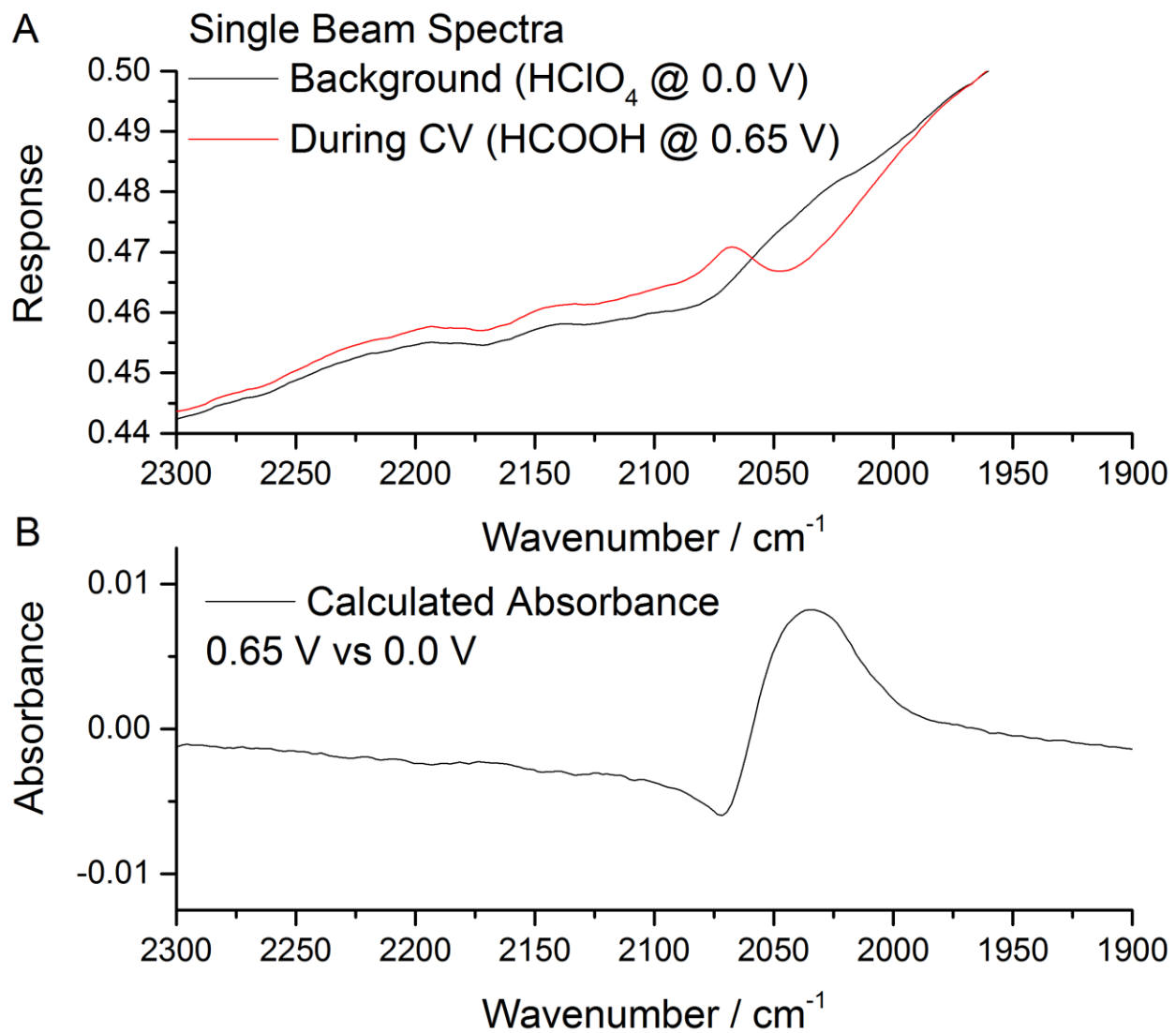


Figure S5 A: Raw single beam spectra before and after addition of HCOOH to show the bipolar nature of the CO absorption. B: Absorption calculated from the two single beam spectra using $A = -\log_{10}(\text{Spectrum during CV} / \text{Background spectrum})$.

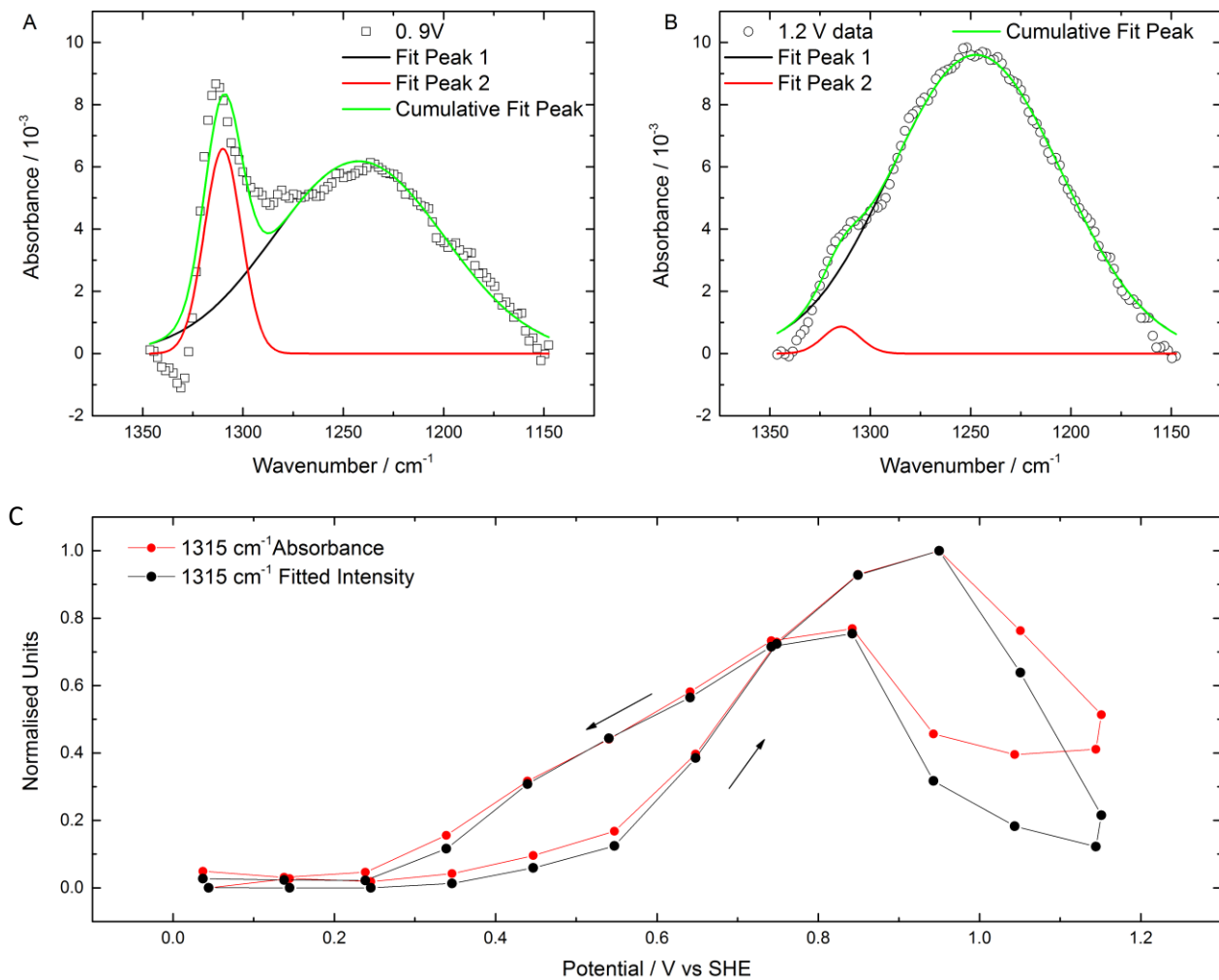


Figure S6 Analysis of the 1315 cm^{-1} peak. A: Raw data at 0.9 V vs SHE from data shown in Figure 2, along with fits using Gaussian functions to represent the 1315 and ca 1250 cm^{-1} peaks. B: As A but at 1.2 V vs SHE. C: Comparison between the potential dependence of the fitted intensity and absorbance of the 1315 cm^{-1} peak. Values have been normalised for comparison through division by the maximum value.

Supplementary References

- [1] K. A. Friedrich, F. Henglein, U. Stimming, W. Unkauf, *Colloids Surf. Physicochem. Eng. Asp.* **1998**, *134*, 193–206.
- [2] V. Stamenković, M. Arenz, P. N. Ross, N. M. Marković, *J. Phys. Chem. B* **2004**, *108*, 17915–17920.
- [3] A. Miki, S. Ye, M. Osawa, *Chem. Commun.* **2002**, 1500–1501.
- [4] H. Miyake, T. Okada, G. Samjeské, M. Osawa, *Phys. Chem. Chem. Phys.* **2008**, *10*, 3662.
- [5] A. Cuesta, G. Cabello, F. W. Hartl, M. Escudero-Escribano, C. Vaz-Domínguez, L. A. Kibler, M. Osawa, C. Gutiérrez, *Catal. Today* **2013**, *202*, 79–86.
- [6] W. Chen, S.-G. Sun, Z.-Y. Zhou, S.-P. Chen, *J. Phys. Chem. B* **2003**, *107*, 9808–9812.
- [7] M. Osawa, in *Adv. Electrochem. Sci. Eng.*, Wiley-VCH Verlag GmbH, Weinheim, Germany, **2006**, pp. 269–314.
- [8] Y. E. Seidel, A. Schneider, Z. Jusys, B. Wickman, B. Kasemo, R. J. Behm, *Langmuir* **2009**, *26*, 3569–3578.
- [9] R. Reichert, J. Schnaitt, Z. Jusys, R. J. Behm, *Phys. Chem. Chem. Phys.* **2014**, *16*, 13780–13799.
- [10] T. J. Smith, K. J. Stevenson, in *Handb. Electrochem.* (Ed.: C.G. Zoski), Elsevier, Amsterdam, **2007**, pp. 73–110.
- [11] S. Park, Y. Xie, M. J. Weaver, *Langmuir* **2002**, *18*, 5792–5798.